Supporting information

for

Nacre tablet thickness records formation temperature in modern and fossil shells

Pupa U.P.A Gilbert[1,2*], Kristin D. Bergmann[3,4], Corinne E. Myers[5,6], Matthew A. Marcus[7], Ross T. DeVol[1], Chang-Yu Sun[1], Adam Z. Blonsky[1], Erik Tamre[2,3], Jessica Zhao[2], Elizabeth A. Karan[2], Nobumichi Tamura[7], Sarah Lemer[5], Anthony J. Giuffre[1], Gonzalo Giribet[5], John M. Eiler[8], Andrew H. Knoll[3,5]

[1] University of Wisconsin–Madison, Departments of Physics, Chemistry, Geoscience, Madison WI 53706 USA.
[2] Harvard University, Radcliffe Institute for Advanced Study, Fellowship Program, Cambridge, MA 02138.
[3] Harvard University, Department of Earth and Planetary Sciences, Cambridge, MA 02138.
[4] Massachusetts Institute of Technology, Department of Earth, Atmospheric and Planetary Sciences, Cambridge, MA 02139.
[5] Harvard University, Museum of Comparative Zoology and Department of Organismic and Evolutionary Biology, Cambridge, MA 02138.
[6] University of New Mexico, Department of Earth and Planetary Sciences, Albuquerque, NM 87131.
[7] Advanced Light Source, Lawrence Berkeley National Laboratory, Berkeley, CA, 94720, USA.
[8] California Institute of Technology, Division of Geological and Planetary Sciences, Pasadena, CA 91125
[*] corresponding author, pupa@physics.wisc.edu, previously publishing as Gelsomina De Stasio

Pinnidae: an ideal family for this study

Specimens within the family Pinnidae, commonly called pen shells or pen clams, were chosen for this study for several reasons. Pinnids are not uncommon in both the modern and fossil records (Figure S1). Thus, modern specimens enabled ground-truthing of the nacre TT-based paleothermometer, and fossil specimens provided a unique window into paleoclimate over 180 Ma of Earth history. Pen shells are large, fast growing bivalves with a thick nacreous region ideal for both spectral and isotopic analyses. Furthermore, the nacre layer in pinnids is easily separated from the prismatic calcite layer. This facilitates sample preparation and minimizes contamination of aragonite nacre with calcite prisms for clumped isotope analysis. Finally, pinnids produce each shell transect in a relatively short period of time, less than a year. Thus comparison with modern shells, grown at known T, makes it possible to identify which shells were primarily deposited in cooler vs. warmer seasons. Anecdote has it that Japanese pearl farmers harvest their pearls in winter, as the tablet thickness is lower, resulting in greater pearl luster (Strack, 2001). This trend in the Japanese pearl bivalve *Pinctada fucata* is similar to that observed in this work for Pinnidae: greater TT at higher T and *vice versa*.

Seven fossil specimens were analyzed for both TT and T, drawn from three locations reflecting warm geologic times and places (the Late Cretaceous Gulf Coastal Plain, ~ 65.5-66 Ma (Landman et al., 2004; Larina, 2015; Thibault and Gardin, 2006, 2007); the Early Eocene Gulf Coastal Plain, ~ 52-54 Ma (Agnini et al., 2007; Frederiksen et al., 1982; Sessa et al., 2012); and the Middle Miocene Mid-Atlantic Calvert Cliffs, ~ 12.7-13.2 Ma) (Kidwell, 1997). In addition, two Jurassic *Pinna* shells were analyzed for TT only, and T was deduced from TT. Many more details are provided in the Pinnidae biology section below.

Pinnidae Biology

The family Pinnidae Leach, 1819 includes subtidal and coastal species (Dance, 2013) found in tropical and temperate regions, both today and in the fossil record. Pinnid species are important elements of certain marine ecosystems, including the sandy substrate of seagrass beds, lagoons and coral reefs where they can sometimes aggregate in large densities (Rosewater, 1961). Pinnids are sessile, suspension-feeding bivalves found partially buried with their anterior end in sand or mud, such that only the posterior prismatic portion of the shell is visible above the sediment (Aucoin and Himmelman, 2011b; Schultz and Huber, 2013; Turner and Rosewater, 1958; Yonge, 1953). The family contains two extant genera and 55 accepted species (although there are more than 16 additional genera in the fossil record) (Lemer et al., 2014; Rosewater, 1961; Schultz and Huber, 2013; Turner and Rosewater, 1958). Pinnids are united by an elongated subtrigonal shell shape, heteromyarian adductor muscle scars (small in the anterior and large in the posterior), a toothless hinge with primary and secondary ligament segments, thin to absent periostracum, byssus, and generally large size (commonly between 15-35cm; Modern *Pinna nobilis* may reach lengths over 1m (Richardson et al., 2004; Schultz and Huber, 2013; Turner and Rosewater, 1958). Pinnidae is nested within the Order Pterioida in Pteriomorphia. However the exact position of Pinnidae and the identity of its sister group remains unclear. Earlier studies based on molecular data have suggested a sister group relationship to Pterioidea, Ostreoidea, or Mytiloidea (Adamkewicz et al., 1997; Bieler et al., 2014; Campbell, 2000; Giribet and Distel, 2003; Giribet and Wheeler, 2002; Matsumoto, 2003; Steiner and Hammer, 2000).

The biomineralized shells of the Pinnidae are composed of an outer calcitic prismatic layer and an inner aragonitic nacreous layer. In pen shells the inner nacreous region does not extend to the posterior margin of the prismatic outer shell, and instead extends from the anterior margin approximately 1/3 to 2/3 the length of the shell (Figure 4). The genera *Pinna* Linnaeus, 1758 and *Atrina* Gray, 1842 may be distinguished by the shape and size of their nacreous layer. In species of the genus *Pinna* the internal nacreous layer is divided by a sulcus into a dorsal and a ventral lobe. The position of the posterior adductor muscle scar with respect to the margins of the nacreous layer is one of the major taxonomic characters used to distinguish species. The posterior adductor muscle scars (PAs in Figure 4) in *Pinna* are fully enclosed within the nacreous region (in the dorsal lobe), whereas in *Atrina* PAs extend to the edge of the nacreous layer, and in some species even beyond the margin into the prismatic portion of the shell (Rosewater, 1982; Schultz and Huber, 2013; Turner and Rosewater, 1958; Yonge, 1953). Finally, in species of the subgenus *Streptopinna* Martens, 1880 (considered a third extant genus until Lemer et al. 2014 (Lemer et al., 2014)) the internal nacreous layer is reduced to a dorsal lobe. The present work focused on species within the extant genera *Atrina* and *Pinna*. These two genera are common in the fossil record and thus provide the most robust history of environmental conditions through time.

Very little is known about the reproductive strategies and the pelagic larval duration of most pinnid species, except for some commercially important ones. Most species are believed to be gonochoristic, to reproduce annually and to produce larvae with a planktotrophic stage with trochophore and veliger stages like *Pinna atropurpurea*, *Atrina pectinata* and *Atrina maura* (Beer and Southgate, 2006; Mendo et al., 2011). Because of their potentially long larval pelagic phase, the dispersal capacity of pinnids is expected to be extensive. This results in a cosmopolitan generic and family distribution, while habitat specificity and past geographic isolation maintained a degree of species-level endemism (e.g. *P. nobilis* in the Mediterranean Sea). Once the veliger settles, the muscular foot is used to bury in soft sediments. Anterior byssus threads then anchor the shell to hard substrate or cobbles in the sediment, such as sea grass beds or coral boulders (Aucoin and Himmelman, 2011a, b; Grave, 1911; Richardson et al., 2004; Rosewater, 1982; Schultz and Huber, 2013; Turner and Rosewater, 1958; Yonge, 1953). Consequently, most species of Pinnidae live within the subtidal photic zone (up to ~ 100 m)(Grave, 1911; Richardson et al., 1999; Schultz and Huber, 2013). Some exceptions exist, e.g., *P. carnea* and other species found in the Pacific Ocean can be found intertidally, and a few species are only found in deep water, down to 600m depth (Schultz and Huber, 2013; Yonge, 1953). Pen shells are fairly delicate, and may be damaged by wave action, currents, storms, or predation (Allen, 2011; Aucoin and Himmelman, 2011b; Grave, 1911; Rosewater, 1982; Turner and Rosewater, 1958; Yonge, 1953). Repair of the prismatic portion of the shell is quite efficient. For instance modern *A. rigida* may repair up to 13mm/day (Grave, 1911), and fully exhumed shells may re-bury themselves. However, successful re-burial is not guaranteed, and exhumation often results in death (Grave, 1911; Richardson et al., 1999; Yonge, 1953).

Growth Rates.—Species of pen shells are some of the fastest growing bivalves known and may grow upwards of 20cm or more radially in their first year of life (Aucoin and Himmelman, 2011b; Butler and Brewster, 1979; Cendejas et al., 1985; Richardson et al., 1999; Richardson et al., 2004). As in most mollusks, faster radial growth occurs early in life;

for pen shells this is generally in the first three years (Butler and Brewster, 1979; Schöne, 2008). Individuals reach reproductive maturity in approximately the second year, and have been known to live up to 20 years in the wild (Aucoin and Himmelman, 2011b; Hendriks et al., 2012; Kožul et al., 2011; Richardson et al., 1999).

Slowdown and even stoppage in radial growth with age has been observed in many mollusk species (e.g. (Schöne, 2008); for species of *Pinna* (Grave, 1911; Hendriks et al., 2012)). Furthermore, both biotic and abiotic environmental factors appear to influence rates of shell growth and stoppages. In addition to age, biotic factors affecting mollusk radial growth rates include: availability of nutrients (food), predation pressure, production of gametes, and spawning (Grave, 1911; Ivany, 2012; Joubert et al., 2014; Linard et al., 2011; Lowenstam and Weiner, 1989; Schöne, 2008). Abiotic factors include: temperature, salinity, lunar cycles and tides, seasonal variations (e.g., day length, storms), turbidity, ocean circulation patterns, sea level, and carbon (organic and inorganic), phosphate, and nitrate concentrations in the water column (Ivany, 2012; Joubert et al., 2014; Linard et al., 2011; Lowenstam and Weiner, 1989; Richardson et al., 1999; Schöne, 2008). Changes in growth rates are commonly detected in bivalves by the deposition of a growth line in the prismatic outer shell (Schöne, 2008). These growth lines, unfortunately, are not produced in species of Pinnidae; however, the posterior adductor muscle scars (PAs in Figure 4) can be used to identify the age of individuals (Butler and Brewster, 1979; Richardson et al., 1999; Richardson et al., 2004). Richardson et al. (Richardson et al., 1999) have documented that PAs from the first year of growth are often absent, thus the age of an individual may be estimated as 1 + number of observed PAs.

Few previous studies have measured slowdowns or stoppages specifically in rates of deposition of the nacreous layer, and none of these were conducted on pen shells. We do not observe any discontinuity in nacre formation for the specimens of *Pinna* and *Atrina* analyzed here (Figure 6), however this does not preclude faster growth seasonally. The most commonly investigated species are those of economic value in pearl aquaculture or human consumption, such as the pearl oyster (*Pinctada margaritifera*) or abalone (e.g., *Haliotis refuscens*). In these few studies, both temperature and nutrient concentrations were observed to impact rates of nacre deposition and total nacre thickness in tank experiments of *P. margaritifera* (Joubert et al., 2014; Linard et al., 2011). Additionally, different suites of genes have been identified in *P. margaritifera* that produce different regulatory proteins for prismatic (radial) vs. nacreous growth (Joubert et al., 2014; Marie et al., 2012). It is very plausible that pen shells, which are closely related to the pearl oysters, share this same genetic framework. Thus, rate of nacre deposition and TT in pen shells may be influenced by abiotic and biotic environmental factors differently than prismatic radial growth, or even continue at a regular rate throughout the life of these species, as the shells of Pinnidae and *Pinctada* thicken significantly after the phase of rapid radial growth (~3 years).

Fossil Record.—The Pinnidae are observed in the fossil record as far back as the Silurian Period (~ 444 Ma) (En-Zhi et al., 1986; Zhang, 1988). A PaleoBiology DataBase (PBDB; paleobiodb.org/) search on 5/25/15 recovered 926 fossil occurrences of *Pinna* and 176 fossil occurrences of *Atrina*, with global distribution (see maps from time periods of interest in Figure S1). *Pinna* first occurs in Middle Mississippian sediments (age range: 345 Ma – present)(Cash, 1882; Wheelton, 1905); *Atrina* is also first observed in the

Carboniferous (age range: ~ 359 Ma – present) (Rosewater, 1961; Ruedemann, 1916, 1918). Although their delicate shells result in difficulty preserving whole body fossils, fragments and partial specimens are not uncommon in warm water, near-shore to offshore paleo-sediments, where their unique morphology makes for easy identification. Further, when preserved in situ, individuals of Pinnidae are often quite abundant in "thickets", akin to modern Mytilidae (Butler and Brewster, 1979; Idris et al., 2008).

DETAILED METHODS

Sample acquisition

We apply a specimen naming convention where the first letter designates the genus, second letter designates the species, and the number indicates the order in which the specimen was received and analyzed. Each sample is further identified by a hyphen and either a "1" (fragment analyzed using PEEM) or "2" (fragment analyzed using clumped isotopes), or greater numbers for additional samples. For example, the *Atrina rigida* specimen was received 5th, thus the PEEM-analyzed sample is labeled: Ar5-1, and the clumped isotope-analyzed sample is labeled Ar5-2. In all figures in this work, however, the last hyphen and number are omitted for simplicity. Associated specimen information is archived in a nacre sample compendium on: http://home.physics.wisc.edu/gilbert/nacre/sample_compendium.html. Table S1 contains a summary of specimen information and Figures 8, 9, S11 provide sample collection location and temperature data measured by nearby buoys or weather stations from the modern samples over the lifetime of the organisms (Pc2, Ar5, and Pn1).

Ar5: Modern *Atrina rigida* (size: 29 cm along the vertical in Figure 4, S4). Purchased from Gulf Specimen Marine Laboratory, Panacea, FL, USA. The living animal was collected at the beginning of September 2014 from St. Joseph Bay, Gulf county, FL (29° 43' 15" N / 85° 19' 39" W) from a collection depth of between 0.5 and 2.0m, kept in a tank for 3-4 weeks, shipped live to Madison, WI and sacrificed on Sept. 30th, 2014. The specimen grew in water temperatures ranging between ~10°C and ~32°C (buoy T data in Figure S11). PEEM sample Ar5-1 was cut from the right valve (RV) of shell Ar5, as shown in Figure S4. Clumped isotope analysis was performed on the left valve (LV) and named Ar_5_a, Ar_5_a_6_10, Ar_5_c. The clumped isotope data from Ar5 were not included because there was major contamination during the analysis, and the results are off by 1000°C.

Ar3: Modern *Atrina rigida* (size: 21 cm). Purchased the same day as Ar5 from Gulf Specimen Marine Laboratory, Panacea, FL, USA. In all other respects identical to Ar5 (see Figure S11 for location and buoy T data). The LV was analyzed here only using SEM in Figure 5, and is therefore not included in Table S1, or in the sample counting.

Pc2: Modern *Pinna carnea* (size: 22.5 cm). Specimen from the Malacology collection of the Museum of Comparative Zoology (MCZ), Harvard University, Cambridge, MA, USA. Catalog number MCZ 382622: collected by Sarah Lemer on March 15, 2015 in Boca del Drago (9°24'17" N / 82°19'26" W), Isla Colón, Archipelago of Bocas del Toro, Panama (Figure 8), at a depth of 1-1.5m. Before sacrificing it, the specimen was kept for six days in an outdoor, shaded tank at the Smithsonian Tropical Research Institute (STRI) Marine station under constant flow of seawater from the coastline at its natural temperature. The specimen grew in water temperatures ranging from ~26°C to ~31°C (Figure 8). The LV was used for both PEEM (Pc2-1) and clumpled isotope (Pc2-2) analyses.

Pn1: Modern *Pinna nobilis* (size: 28 cm). Also from the Malacology collection of the MCZ, Harvard University, Cambridge, MA, USA. Catalog number MCZ 371544: collected by Juan Giribet in Mallorca, Spain, 1991 (Figure 9). The temperature record from 1990-1991 is unavailable. Temperature records in Figure 9 show the locations where the buoy T data were collected in recent years. The specimen likely grew in water temperatures ranging from ~10°C to ~30°C (Figure 9). The LV was used for both PEEM (Pn1-1) and clumped isotopes (Pn1-2) analyses.
Ah2: Miocene *Atrina harrisii* (fragment size: 7 cm). Courtesy of Robert Hazen and John Nance, Calvert Marine Museum Invertebrates Collection, Solomons, MD USA. Catalogue number CMM-I-237: collected from Bed 19, Boston Cliffs Member, Choptank Formation, Chesapeake Group (Middle Miocene Epoch ~12 Ma). The sample appearance and preparation are shown in Figure S7. Fragment size prohibited identification of RV or LV for PEEM (Ah2-1) and clumped isotope (Ah2-2) analyses but both analyses were conducted on the same fragment.
Ah3: Miocene *Atrina harrisii* (fragment size: 4.5 cm). Courtesy of Susan Butts and Jessica Utrup, Yale Peabody Museum (YPM), Yale University, New Haven, CT, USA. Catalogue number IP 527493: collected by S. M. Kidwell in Saint Marys Co, MD in 1979. Specimen collected from Unit 5 of the Drumcliff Member, Choptank Formation (Middle Miocene ~13 Ma). For more information, see: http://peabody.yale.edu/collections/search-collections?ip. A single fragment (RV/LV unknown) was used for PEEM (Ah3-1) and clumped isotope (Ah3-2) analyses. Species designation determined by the authors and confirmed by John Nance (Calvert Marine Museum of Invertebrates) based on absence of interior sulcus or exterior keel, and comparison to other age-equivalent specimens previously described from the Drumcliffs Member (Glenn, 1904; Kidwell, 1982).
Ah4: Miocene *Atrina harrisii* (fragment size: 5.5 cm). Courtesy of Susan Butts and Jessica Utrup, YPM, Yale University, New Haven, CT, USA. Catalogue number IP 527512: collected by S. M. Kidwell in Saint Marys Co, MD in 1978. Specimen collected from the top of Unit 1, Drumcliff Shell Bed, Choptank Formation (Middle Miocene ~13 Ma). For more information, see: http://peabody.yale.edu/collections/search-collections?ip. A single fragment (RV/LV?) was used for PEEM (Ah4-1) and clumped isotope (Ah4-2) analyses. Species designation determined by the authors and confirmed by John Nance (Calvert Marine Museum of Invertebrates) based on absence of interior sulcus or exterior keel, and comparison to other age-equivalent specimens previously described from the Drumcliffs Member (Glenn, 1904; Kidwell, 1982).
Px1: Eocene cf. *Pinna* sp., (fragment size: 3.5 cm). Courtesy of Susan Butts and Jessica Utrup, YPM, Yale University, New Haven, CT, USA. Catalogue number IP 527489: collected by C. O. Dunbar on Feb. 4, 1966 in Butler Co, AL (Coll. 3). Specimen collected from the Bashi Shell Marl, lower Hatchetigbee Formation (Early Eocene ~54 Ma). For more information, see: http://peabody.yale.edu/collections/search-collections?ip. A single fragment (RV/LV?) was used for PEEM (Px1-1) and clumped isotope (Px1-2) analyses.
Px2: Eocene cf. *Pinna* sp. (fragment size: 6 cm). Courtesy of Susan Butts and Jessica Utrup, YPM, Yale University, New Haven, CT, USA. Catalogue number IP 527490: collected by C. O. Dunbar on Feb. 4, 1966 in Butler Co, AL (Coll. 3). Specimen collected from the Bashi Shell Marl, lower Hatchetigbee Formation (Early Eocene ~54 Ma). For more information, see: http://peabody.yale.edu/collections/search-collections?ip . A single fragment (RV/LV?) was used for PEEM (Px2-1) and clumped isotope (Px2-2) analyses.

Ps5: Late Cretaceous (Maastrichtian) *Pinna* sp. (fragment size: 8 cm). Courtesy of Neil Landman and Bushra M. Hussaini, American Museum of Natural History (AMNH), New York, NY, USA. Catalogue number 99982: collected by Neil Landman, Susan Klofak, Matt Garb, Remy Rovelli, and Corinne Myers on May 28, 2010 in Tippah, Co, MS. Specimen collected from the Owl Creek Fm, Selma Group (Maastrichtian ~66 Ma). Accessioned specimen consists of many shell fragments; two separate fragments were used for Ps5 and Ps6 below. A single fragment (RV/LV?) was used for PEEM (Ps5-1), clumped isotope (Ps5-2a, Ps5-2c), and EPMA (Ps5-4) analyses. By comparison with *Pinna laqueata* specimens found at this site at the same time and those previously observed in the Owl Creek of Missouri (Stephenson, 1957), it is possible that this shell species was *Pinna laqueata*.
Ps6: Late Cretaceous (Maastrichtian) *Pinna* sp. (fragment size: 4 cm). Courtesy of Neil Landman and Bushra M. Hussaini, AMNH, New York, NY, USA. Specimens from same catalogue number, locality, and stratigraphic interval as Ps5 above. A single fragment (RV/LV?) was used for PEEM (Ps6-1) and clumped isotope (Ps6-2a, Ps6-2c) analyses. As for Ps5, it is possible that Ps6 is *Pinna laqueata*, as other *P. laqueata* specimens were found at this site (Stephenson, 1957).
Pfo1: Early Jurassic (Pliensbachian) *Pinna folium* (remaining shell size: 12 cm, estimated total size including missing umbo: 15 cm), from Blockley, Gloucestershire, UK, extracted from the Lower Lias. Courtesy of Steven Davies, Dinosaurland Fossil Museum collection, Lyme Regis, Dorset, United Kingdom. The shell shows excellent iridescence, and does not have any calcite prismatic layer in the areas analyzed with SEM. It does not have the umbo anymore. The two valves are closed and filled with calcite, identified by PEEM analysis. A 1cm thick slice was embedded and cut as close to the umbo as possible (~3 cm from it), embedded, polished, and analyzed with SEM. The best region (position 3) was cut, re-embedded and polished for PEEM analysis (Pfo1-3)(Figure S8). No clumped isotope analysis was done as this specimen occluded extensive calcite crystals between the two valves (see top of transects in Figure 6), and the nacre layer was too thin (300 µm at most) for safe, uncontaminated separation.
Ps8: Early Jurassic (Pliensbachian) *Pinna folium* (remaining shell size: 5.6 cm, estimated total size including missing umbo: 7 cm), from Blockley, Gloucestershire, UK, extracted around the year 2000 from the Northcott Brick works, Ibex zone, *Beanicerus luridum*. Courtesy of Christopher Andrew, Lyme Regis Museum, Lyme Regis, Dorset, United Kingdom. The shell shows limited iridescence only in one region, and from SEM and PEEM analysis does not have any calcite prismatic layer preserved. It does not have the umbo anymore. The two valves are closed and filled with polycrystalline calcite (from PEEM analysis), the entire specimen was embedded, cut, polished, and analyzed with SEM. The best region (position 2) was cut, re-embedded and polished for PEEM analysis (Ps8-2)(Figure S8). No clumped isotope analysis was done as this specimen had extensive calcite crystals between the two valves, outside of the nacre layer, in between the nacre layer, and even percolating through some of the nacre tablets (see Figure 2F). The nacre layer was even thinner than in the Pfo sample, with 90 µm maximum thickness.

Sample preparation

Three modern and seven fossil specimens were acquired from the sources described above. The three modern shells were rinsed in ethanol, air-dried, and cut with a

jeweler's saw along the bisector line. A second cut, shown in Figure S4b, isolated a shell fragment ~1cm-wide including the thickest nacre (red arrows in Figures 4, S4, S7) at its center. This sample was then embedded in epoxy to expose the cross-section in the thickest nacre region, polished, and coated. The thickest nacre region was chosen because it provides the most sample to measure, and was deposited over the longest period of time. Consequently, experiments in this region maximize the environmental information stored in each specimen.

Fossil Pinnidae shells are extremely fragile, as shown by the shell fragments at the right hand side of Figure S7a,b for specimen Ah2. These fragments were cut off for clumped isotope analysis using a razor blade gently pressed through the soft, flaky nacre. Subsequently the remaining specimen was embedded in epoxy, then cut using a diamond saw as shown in Figures S6 and S7c,d. Fossil specimens were then re-embedded to expose a shell cross-section in the region of thickest nacre (missing cuboid in Figure S6 and S7c,d), polished, and coated similar to modern specimens.

The embedding epoxy in all cases was EpoFix (EMS, Hatfiled, PA, USA), poured around the shell fragment in 1-inch round molds, and cured for 13 hours. Before embedding, extreme care was taken to coarsely polish each shell to obtain a flat cross-section perpendicular to the shell inner surface. The specimen was then mounted on double-stick tape to the bottom of the embedding mold in order to minimize any orientation error introduced during the embedding stage. The finished shell mount contained nacre layers perpendicular to the polished surface within an angle of ±5°, thus the mounting error on TT measurements was negligible.

Shell mounts were polished with coarse grit, followed by 300-nm Al_2O_3 nanoparticles, followed by 50-nm Al_2O_3 nanoparticles (MasterPrep, Buehler, Lake Bluff, IL, USA) suspensions. Before use, both polishing suspensions were dialyzed against 22g/L Na_2CO_3 in DD water for 24h with three Na_2CO_3 solution changes. The polished samples were rinsed in ethanol, air-dried, covered with a mask in the area to be analyzed (purple square in Figure S4d, transparent square in Figure S7e,) and coated with 40nm Pt. This produced the high-reflectivity region all around the square, (the white region in Figure S4d and black region in Figure S7e). The mask was then removed, and the entire sample surface was coated again with 1nm Pt, while rotating the sample. One nm is sufficient to ensure good conductivity, but is less than the ~5 nm depth below the sample surface from which the secondary electrons detected in a PEEM experiments originate (Frazer et al., 2003). Hence the majority of the detected signal comes from the sample, not the coating. One nm Pt, however, is not enough to make good electrical contact, motivating the thicker coating surrounding the area of interest. One nm coating must be done using a high-precision sputter coater that enables slow, precise coating, during which the sample is tilted and spun (208HR High Resolution Sputter Coater, Cressington, UK, and Ted Pella, Inc., USA). The differential-thickness resulting from two rounds of Pt coating makes it possible to perform photoemission experiments on shells, minerals, rocks, or any other insulators, and was introduced by our group (De Stasio et al., 2003; DeVol et al., 2014). It also prevents any charging phenomena or artifacts (Gilbert et al., 2000). Figure S7e shows a polished, trimmed, and coated sample, ready for PEEM analysis.

Sample powders were prepared for clumped isotope analyses from the epoxy-embedded shell fragments surrounding the PEEM sub-sample for Ah3-2, Ah4-2, Px1-2 and Px2-2. A bulk sample of nacre was removed from the epoxy and powdered using a mortar

and pestle. For Ah2-2, a subsample from the fragments produced while cutting the sample with a razorblade was powdered with a mortar and pestle. Unembedded samples of Ar5, Pc 1-2, Pn 2-2, Pl-5-2 and Pl-6-2 allowed separation of the prismatic calcite layer and the nacre using a razor blade. Both were powdered using a mortar and pestle prior to clumped isotope analysis.

XRD Analysis

X-ray diffraction patterns (XRD) were collected on beamline 12.3.2 at the Berkeley Advanced Light Source, as described previously, using a DECTRIS Pilatus 1 M area detector (Gilbert et al., 2008; Tamura and Gilbert, 2013; Yang et al., 2011). A ~1-μm spot, 9 keV monochromatic beam illuminated the sample surface in the locations shown in Figure S2. Each pattern of reflections was indexed using the XMAS software (Tamura, 2014) , with excellent calcite and aragonite recognition.

SEM Analysis

For scanning electron microscopy (SEM) analysis, the anterior regions of three modern shells were cut, rinsed with ethanol, air-dried, and coated with 20-nm Pt. The Hitachi S-3400N scanning electron microscope in the UW-Madison Department of Geoscience was used to produce the images in Figure 5, under the secondary-electron mode and an accelerating voltage of 15 kV.

EPMA analysis

Electron Probe Micro-Analysis (EPMA) was conducted to obtain quantitative elemental spot analysis and elemental mapping on the shell Ps 5-4 to assess trace metal variability across the shell. EPMA was done on the JEOL JXA-8200 Electron Microprobe at the California Institute of Technology. For all quantitative results, the accelerating voltage was 15 kV, the beam current was 20 nA, and the beam size was 1 μm. The CITZAF method was used for matrix correction. Sample standards for the five chemical elements analyzed, included: dolomite for Mg, siderite for Fe, rhodochrosite for Mn, strontianite for Sr, and anhydrite for S. Mg had an average detection limit of 0.01% Fe–272 ppm, Mn–388 ppm, Sr–438 ppm, and S–0.02%. EPMA results are presented in Figure S3 and reported in Table S3. The Late Cretaceous shell Ps5 is also extremely well preserved chemically. EPMA measurements, both maps and transects, indicate that Fe and Mn trace metal concentrations are extremely low across the shell (aragonite [Fe] = 110 ± 12 ppm and [Mn] = 90 ± 10 ppm; calcite [Fe] = 202 ± 42 ppm and [Mn] = 93 ± 27 ppm, mean ± std. error of the mean). As both metals tend to incorporate into calcite and aragonite in reducing environments below the sediment-water interface, this suggests minimal diagenesis (Brand and Veizer, 1980). Sr and Mg are consistent with primary precipitation of the two phases from seawater (aragonite [Sr] = 2567 ± 71 ppm and [Mg] = 134 ± 33 ppm; calcite [Sr] = 986 ± 38 ppm and [Mg] = 3909 ± 187 ppm) (Figure S3, Table S3).

Detailed description of digital ruler measurements

Each PIC-map was opened in Adobe Photoshop®, then immediately duplicated into a second "Photoshop layer". This second layer was then rotated until the nacre tablets were horizontal. Tilt in the other direction was prevented with accurate sample mounting, perpendicular to the polishing and imaging plane. A vertical un-rotated digital ruler with

ticks and numbers was pasted into a third "Photoshop layer". For all images, the digital ruler was arranged such that the "0" tick was located precisely at the bottom of the un-rotated PIC-map. All other ticks were then moved so that each coincided with the boundary between two nacre tablets. In Figure S9 the three "Photoshop layers" are displayed for each PIC-map: at the bottom is the un-rotated original PIC-map layer, on top of it is the rotated PIC-map, and on top of both is the digital ruler, with its white ticks and numbers. Note that "0" is at the bottom of the field of view, and all other ticks and numbers were shifted up or down, one at a time, such that they coincided with nacre tablet boundaries. The vertical-FoV was 21.5 μm in all panels of Figure S9. Note that in Figure S9 we displayed a larger field of view to include all of the un-rotated images. During the measurement the file size was not (and should not be) increased, so the FoV measurement remained the same, even when a Photoshop layer was rotated. This avoids the introduction of any quantitative errors. To obtain the "average TT" in each PIC-map (Figure S10) we divided the vertical-FoV in each image by the number of tablets counted in that image using the digital ruler. All PIC-maps were measured twice, by two co-authors, recording the results in two separate columns of a Microsoft Excel® spreadsheet. The averages and standard deviations were calculated in Excel®, all the plots were produced in Kaleidagraph® 4.5.2 for Mac.

Angle spread measurement

The angle spread of c'-axes (the projections of c-axes onto the polarization plane of the illuminating radiation) was measured using the "Polarization Analysis Package" of GG Macros (GG–Macros, 2016). For every PIC-mapped area, we made a polarization stack of 19 images, with linearly polarized illumination covering a range of 90° with a 5° step. By fitting the intensity of a pixel as a function of polarization to Equation 1 (see PIC-mapping), we then determined the values of *c'*, the c'-axis angle, and *b*, the amplitude of polarization-dependent intensity, for every pixel in a PIC-mapped area.

To remove artifacts before measurement, we first masked off pixels with extreme values of *b*, namely those falling into bins populated by less than 10^2 pixels on a histogram of all *b*-values from the PIC-map. In particular, this removes artifacts with low polarization-dependence and correspondingly low values of *b*.

We then placed the *c'*-values of all remaining pixels on a histogram and measured the range of these c'-axis angle bins that were each occupied by at least 10^3 pixels. This somewhat arbitrary occurrence cut-off was used to further ensure that remaining c'-axis angles, still representing the majority of the 10^6 pixels in the image, are not artifactual. Great care was taken to confirm that no real nacre tablets were completely excluded from the AS analysis by this cut-off. The measured angle spread in each PIC-map was always between 10° and 30° for all areas analyzed in modern and fossil nacre, with the only six exceptions due to diagenesis and shown in the six panels of Figure 2.

Using the GG Macros (GG–Macros, 2016), this analysis of a given PIC-map can be done by following a few simple steps:

1) Having opened the experiment file, stacked the 19 images, and produced a PIC-map, now click on the "Analyze output" button in the "Polarization Panel".
2) The "Polarization Result Analysis" panel appears. In that panel, press "Create Masked PICmap". When you do that, make sure that box "From POL B" is checked in the "Masking"

section of the panel: that masks off pixels with extreme *b*-values, with <10^3 frequency, as described above.
3) A histogram of *c'*-values of unmasked pixels appears. Check that the vertical cut-offs are placed at the 10^3 level; if necessary, move them manually.
4) Click on "Extract Masked AS". The angle spread is measured and displayed in the command panel.

The average angle spread thus obtained for each shell is shown in Figure S13, and, although extremely noisy, it appears to be anti-correlated with T. It is possible that this is a sampling artifact: at greater T tablet thickness is greater, hence there are fewer tablets in the field of view and their possible orientations are under-sampled, resulting in smaller angle spreads. This is confirmed by the shape of *c'*-value histograms, which significantly departs from Gaussian at higher T, and is generally closer to Gaussian at lower T. Rather than the angle spread in each PIC-map, a measurement of all orientation angles over the entire shell might be more informative, but is beyond the scope of this work.

2.7 Abiotic aragonite growth experiment
Aragonite growth.—Synthetic aragonite particles were grown simultaneously in sealed Pyrex bowls placed in bio-culture rooms or incubators with different temperatures. The growth solution recipe follows (Liu et al., 2009). Four 22 mm × 22 mm glass coverslips were each placed in a 35mm plastic Petri dish containing 3 ml of 10mM $CaCl_2$ + 10mM $MgCl_2$. Petri dishes were covered and sealed with Al foil surrounded by Parafilm. Four holes were poked in the Al foil of each dish, using a needle. Each of four covered Petri dishes was placed in a separate sealable 950 ml Pyrex bowl. A chunk of ammonium carbonate (~8-9 g) was placed on a 35 mM Petri dish with no cover, and put in each of the Pyrex bowls. The Pyrex bowls were then sealed with plastic covers, and placed in a bowl at one of four different temperatures: 4°C, 15°C, 22°C, and 30°C (4°C and 15°C = "cold" room; 22°C = lab room temperature; 30°C = bacteria plate incubator set to 30°C.). Twenty hours later, each glass coverslip was removed from the growth solution with forceps and rinsed in 10mM Tris, pH 11 for a few seconds, rinsed in 100% ethanol for about 5 seconds, and placed in clean 35mm Petri dishes at an angle resting on the lip of the dish to dry for 1 hour. Dry coverslips were then placed in labeled 50ml screw cap tubes containing Kimwipes to hold the coverslips in place, and transported for imaging.
Particle size measurement.—Each coverslip with aragonite particles was imaged using crossed polarizers in reflection mode on a Nikon MM400 visible light microscope. The larger particles grown at 15, 22, 30°C were imaged using the smallest magnification (5× objective); the 4°C-particles were imaged with the highest magnification (100× objective). Fifteen or more image files were acquired and saved from each sample. Aragonite crystal diameters were measured in Image J® using the "straight line selection" tool, after setting the scale to the appropriate magnification. The green lines shown in Figure 10 were drawn in Adobe Photoshop® in locations similar to those selected for measurement in Image J®.

Supporting Information References
Adamkewicz, S.L., Harasewych, M., Blake, J., Saudek, D., Bult, C.J., 1997. A molecular phylogeny of the bivalve mollusks. Molec biol Evol 14, 619-629.

Agnini, C., Fornaciari, E., Raffi, I., Rio, D., Röhl, U., Westerhold, T., 2007. High-resolution nannofossil biochronology of middle Paleocene to early Eocene at ODP Site 1262: implications for calcareous nannoplankton evolution. Marine Micropaleont 64, 215-248.
Allen, J.A., 2011. On the functional morphology of Pinna and Atrina larvae (Bivalvia: Pinnidae) from the Atlantic. J Marine Biol Assoc UK 91, 823-829.
Aucoin, S., Himmelman, J., 2011a. Factors determining the abundance, distribution and population size–structure of the penshell Pinna carnea. Journal of the Marine Biological Association of the United Kingdom 91, 593-606.
Aucoin, S., Himmelman, J., 2011b. Factors determining the abundance, distribution and population size–structure of the penshell Pinna carnea. J Marine Biol Assoc UK 91, 593-606.
Beer, A.C., Southgate, P.C., 2006. Spat collection, growth and meat yield of Pinna bicolor (Gmelin) in suspended culture in northern Australia. Aquaculture 258, 424-429.
Bieler, R., Mikkelsen, P.M., Collins, T.M., Glover, E.A., González, V.L., Graf, D.L., Harper, E.M., Healy, J., Kawauchi, G.Y., Sharma, P.P., 2014. Investigating the Bivalve Tree of Life–an exemplar-based approach combining molecular and novel morphological characters. Invert Systemat 28, 32-115.
Brand, U., Veizer, J., 1980. Chemical diagenesis of a multicomponent carbonate system--1: Trace elements. J Sedim Res 50, 1219-1236.
Butler, A., Brewster, F., 1979. Size distributions and growth of the fan-shell *Pinna bicolor* Gmelin (Mollusca: Eulamellibranchia) in South Australia. Marine Freshwater Res 30, 25-39.
Campbell, D.C., 2000. Molecular evidence on the evolution of the Bivalvia. Geol Soc Lond Spec Publ 177, 31-46.
Cash, W., 1882. Yorkshire Fossil Mollusca, Proceedings of the Yorkshire Geological and Polytechnic Society. Geological Society of London, pp. 77-88.
Cendejas, J., Carvallo, M., Juárez, L., 1985. Experimental spat collection and early growth of the pen shell, Pinna rugosa (Pelecypoda: Pinnidae), from the Gulf of California. Aquaculture 48, 331-336.
Dance, S.P., 2013. The encyclopedia of shells.
De Stasio, G., Frazer, B.H., Gilbert, B., Richter, K.L., Valley, J.W., 2003. Compensation of charging in X-PEEM: a successful test on mineral inclusions in 4.4 Ga old zircon. Ultramicroscopy 98, 57-62.
Dennis, K.J., Affek, H.P., Passey, B.H., Schrag, D.P., Eiler, J.M., 2011. Defining an absolute reference frame for 'clumped'isotope studies of CO 2. Geochim Cosmochim Acta 75, 7117-7131.
DeVol, R.T., Metzler, R.A., Kabalah-Amitai, L., Pokroy, B., Politi, Y., Gal, A., Addadi, L., Weiner, S., Fernandez-Martinez, A., Demichelis, R., Gale, J.D., Ihli, J., Meldrum, F.C., Blonsky, A.Z., Killian, C.E., Salling, C.B., Young, A.T., Marcus, M.A., Scholl, A., Doran, A., Jenkins, C., Bechtel, H.A., Gilbert, P.U.P.A., 2014. Oxygen spectroscopy and Polarization-dependent Imaging Contrast (PIC)-mapping of calcium carbonate minerals and biominerals. J Phys Chem B 118, 8449-8457.
En-Zhi, M., Boucot, A., Xu, C., Jia-Yu, R., 1986. Correlation of the Silurian rocks of China. Geol Soc Amer Special Papers 202, 1-81.
Frazer, B.H., Gilbert, B., Sonderegger, B.R., De Stasio, G., 2003. The probing depth of total electron yield in the sub keV range: TEY-XAS and X-PEEM. Surf Sci 537, 161-167.
Frederiksen, N.O., Gibson, T.G., Bybell, L.M., 1982. Paleocene-Eocene boundary in the eastern Gulf Coast. Gulf Coast Assocn Geol Soc Trans 32, 289-294.

GG–Macros, 2016. http://home.physics.wisc.edu/gilbert/GG-macros.
Gilbert, B., Andres, R., Perfetti, P., Margaritondo, G., Rempfer, G., De Stasio, G., 2000. Charging phenomena in PEEM imaging and spectroscopy. Ultramicroscopy 83, 129-139.
Gilbert, P.U.P.A., Metzler, R.A., Zhou, D., Scholl, A., Doran, A., Young, A., Kunz, M., Tamura, N., Coppersmith, S.N., 2008. Gradual Ordering in Red Abalone Nacre. J Am Chem Soc 130, 17519-17527.
Giribet, G., Distel, D.L., 2003. Bivalve phylogeny and molecular data. Molec System Phylogeogr Moll, 45-90.
Giribet, G., Wheeler, W., 2002. On bivalve phylogeny: a high‐level analysis of the Bivalvia (Mollusca) based on combined morphology and DNA sequence data. Invert Biol 121, 271-324.
Glenn, L., 1904. Mollusca, Pelecypoda. System Paleontol Miocene: Maryland Geological Survey Miocene Volume, 274-401.
Grave, B.H., 1911. Anatomy and physiology of the wing-shell *Atrina rigida*. Govt. print. off.
Hendriks, I.E., Basso, L., Deudero, S., Cabanellas-Reboredo, M., Álvarez, E., 2012. Relative growth rates of the noble pen shell Pinna nobilis throughout ontogeny around the Balearic Islands (Western Mediterranean, Spain). J Shellfish Res 31, 749-756.
Idris, M., Arshad, A., Bujang, J., Ghaffar, M., Daud, S., 2008. Biodiversity and distribution of pen shells (Bivalvia: Pinnidae) from the seagrass beds of Sungai Pulai, Peninsular Malaysia. Res J Fisheries Hydrobiol 3, 54-62.
Ivany, L.C., 2012. Reconstructing paleoseasonality from accretionary skeletal carbonates—challenges and opportunities, Reconstructing Earth's Deep-Time Climate—The State of the Art in 2012, pp. 133-165.
Joubert, C., Linard, C., Le Moullac, G., Soyez, C., Saulnier, D., Teaniniuraitemoana, V., Ky, C.L., Gueguen, Y., 2014. Temperature and Food Influence Shell Growth and Mantle Gene Expression of Shell Matrix Proteins in the Pearl Oyster Pinctada margaritifera. PloS one 9, e103944.
Kidwell, S.M., 1982. Stratigraphy, in Vertebrate Taphonomy and Depositional History of the Miocene Calvert and Choptank Formations, Atlantic Coastal Plain. Yale University.
Kidwell, S.M., 1997. Anatomy of extremely thin marine sequences landward of a passive-margin hinge zone: Neogene Calvert Cliffs succession, Maryland, USA. J Sedim Res 67, 322-340.
Kožul, V., Glavić, N., Bolotin, J., Antolović, N., 2011. The experimental rearing of fan mussel Pinna nobilis (Linnaeus, 1758), Procs 46th Croatian and 6th Internat Symp on Agriculture, Opatija, Croatia, p. 806.
Landman, N.H., Johnson, R.O., Edwards, L.E., 2004. Cephalopods from the Cretaceous/Tertiary boundary interval on the Atlantic Coastal Plain, with a description of the highest ammonite zones in North America. Part 2. Northeastern Monmouth County, New Jersey. Bull Am Mus Nat Hist 287, 1-107.
Larina, E.A., 2015. Upper Maastrictian ammonite biostratigraphy of the Gulf Coastal Plain, Geology. Brooklyn College, p. 65.
Lemer, S., Buge, B., Bemis, A., Giribet, G., 2014. First molecular phylogeny of the circumtropical bivalve family Pinnidae (Mollusca, Bivalvia): evidence for high levels of cryptic species diversity. Molec phylog evol 75, 11-23.

Linard, C., Gueguen, Y., Moriceau, J., Soyez, C., Hui, B., Raoux, A., Cuif, J.P., Cochard, J.-C., Le Pennec, M., Le Moullac, G., 2011. Calcein staining of calcified structures in pearl oyster Pinctada margaritifera and the effect of food resource level on shell growth. Aquaculture 313, 149-155.
Liu, R., Xu, X., Cai, Y., Cai, A., Pan, H., Tang, R., Cho, K., 2009. Preparation of calcite and aragonite complex layer materials inspired from biomineralization. Cryst Growth Des 9, 3095-3099.
Lowenstam, H.A., Weiner, S., 1989. On biomineralization. Oxford University Press.
Marie, B., Joubert, C., Tayalé, A., Zanella-Cléon, I., Belliard, C., Piquemal, D., Cochennec-Laureau, N., Marin, F., Gueguen, Y., Montagnani, C., 2012. Different secretory repertoires control the biomineralization processes of prism and nacre deposition of the pearl oyster shell. Proc Natl Acad Sci USA 109, 20986-20991.
Matsumoto, M., 2003. Phylogenetic analysis of the subclass Pteriomorphia (Bivalvia) from mtDNA COI sequences. Molec Phylogen Evol 27, 429-440.
Mendo, T., Koch, V., Wolff, M., Sínsel, F., Ruiz-Verdugo, C., 2011. Feasibility of intertidal bottom culture of the penshell Atrina maura in Bahia Magdalena, Baja California Sur, Mexico. Aquaculture 314, 252-260.
Richardson, C., Kennedy, H., Duarte, C., Kennedy, D., Proud, S., 1999. Age and growth of the fan mussel *Pinna nobilis* from south-east Spanish Mediterranean seagrass (*Posidonia oceanica*) meadows. Marine Biol 133, 205-212.
Richardson, C., Peharda, M., Kennedy, H., Kennedy, P., Onofri, V., 2004. Age, growth rate and season of recruitment of *Pinna nobilis* (L) in the Croatian Adriatic determined from Mg: Ca and Sr: Ca shell profiles. J Exper Marine Biol Ecol 299, 1-16.
Rosewater, J., 1961. The family Pinnidae in the Indo-Pacific. Indo-Pacif Mollusca 1, 501.
Rosewater, J., 1982. Review of Hawaiian Pinnidae and revalidation of Pinna exquisita Dall, Bartsch, and Rehder, 1938 (Bivalvia: Mytiloida).
Ruedemann, R., 1916. The Paleontology of Arrested Evolution. New York State Mus Bull 196, 107-134.
Ruedemann, R., 1918. The Paleontology of Arrested Evolution: Address by the President of the Paleontological Society, Albany, December 1916. University of the State of New York.
Schöne, B.R., 2008. The curse of physiology—challenges and opportunities in the interpretation of geochemical data from mollusk shells. Geo-Marine Lett 28, 269-285.
Schultz, P.W., Huber, M., 2013. Revision of the worldwide recent Pinnidae and some remarks on fossil European Pinnidae. ConchBooks, Öhringen, Germany.
Sessa, J.A., Ivany, L.C., Schlossnagle, T.H., Samson, S.D., Schellenberg, S.A., 2012. The fidelity of oxygen and strontium isotope values from shallow shelf settings: Implications for temperature and age reconstructions. Palaeogeogr Palaeoclimatol Palaeoecol 342, 27-39.
Steiner, G., Hammer, S., 2000. Molecular phylogeny of the Bivalvia inferred from 18S rDNA sequences with particular reference to the Pteriomorphia. Geol Soc Lond Spec Publ 177, 11-29.
Stephenson, L.W., 1957. A shorter contribution to general geology. Geol Survey Profess Paper 274, 97.
Strack, E., 2001. Pearls. Rühle-Diebener Verlag, Stuttgart. ISBN 3-00-008636-6.
Tamura, N., 2014. XMAS: A versatile tool for analyzing synchrotron X-ray microdiffraction data. Strain and Dislocation Gradients from Diffraction. Spatially-Resolved Local Structure and Defects; Barabash, R, 125-155.

Tamura, N., Gilbert, P.U.P.A., 2013. X-ray Microdiffraction of Biominerals, in: De Yoreo, J.J. (Ed.), Research Methods in Biomineralization Science Academic Press, Burlington, MA, pp. 501-532.
Thibault, N., Gardin, S., 2006. Maastrichtian calcareous nannofossil biostratigraphy and paleoecology in the Equatorial Atlantic (Demerara Rise, ODP Leg 207 Hole 1258A). Rev Micropaléontol 49, 199-214.
Thibault, N., Gardin, S., 2007. The late Maastrichtian nannofossil record of climate change in the South Atlantic DSDP Hole 525A. Marine Micropaleontol 65, 163-184.
Turner, R.D., Rosewater, J., 1958. The family Pinnidae in the western Atlantic. Johnsonia 3, 285-326.
Wheelton, H., 1905. A monograph of the British Carboniferous Lamellibranchiata Volume II. Palaeontographical Society.
Yang, L., Killian, C.E., Kunz, M., Tamura, N., Gilbert, P.U.P.A., 2011. Biomineral nanoparticles are space-filling. RSC-Nanoscale 3, 603-609.
Yonge, C.M., 1953. Form and habit in Pinna carnea Gmelin. Philosophical Transactions of the Royal Society B: Biological Sciences 237, 335-374.
Zhang, R., 1988. Stratigraphic and paleobiogeographic aspects of Devonian bivalves of China.

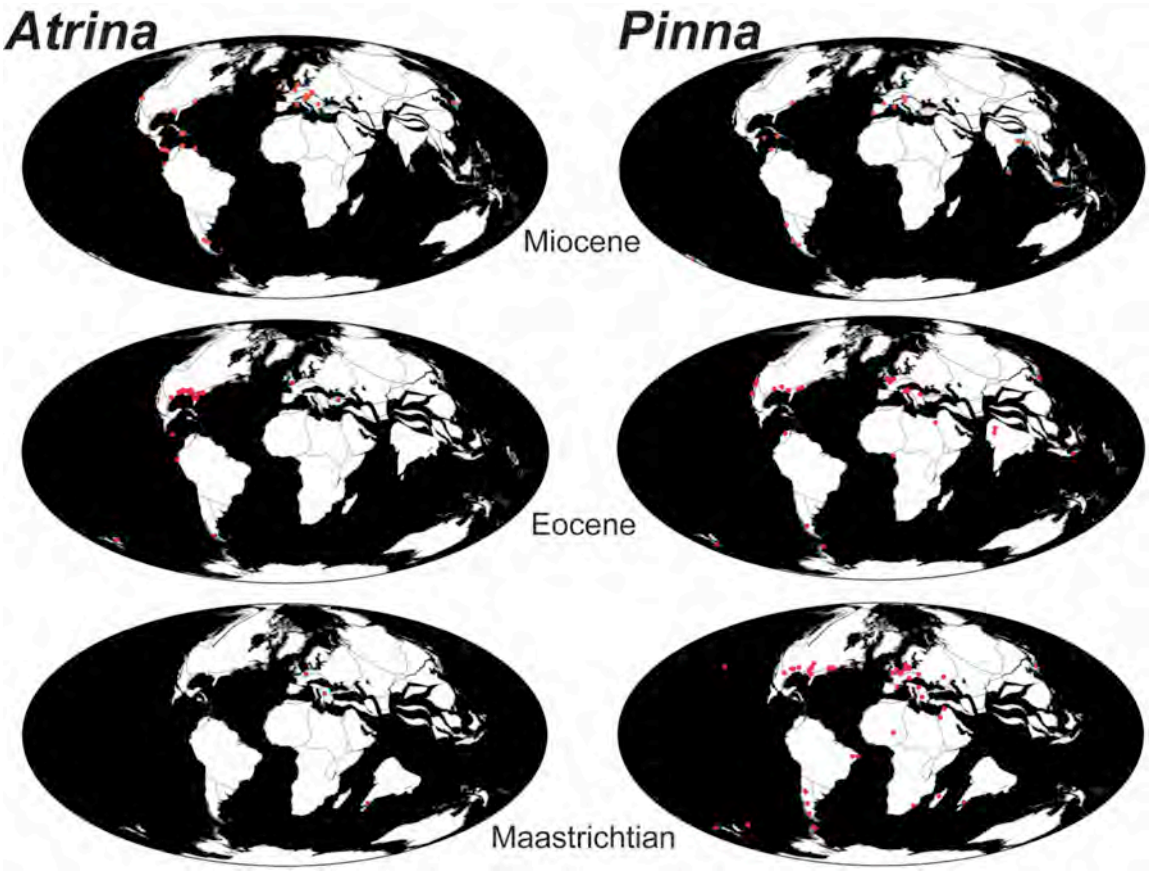

Figure S1. Fossil distribution of *Atrina* and *Pinna* during the Miocene, Eocene, and Late Cretaceous epochs. Fossil occurrence data downloaded from the Paleobiology Database on 5/25/15.

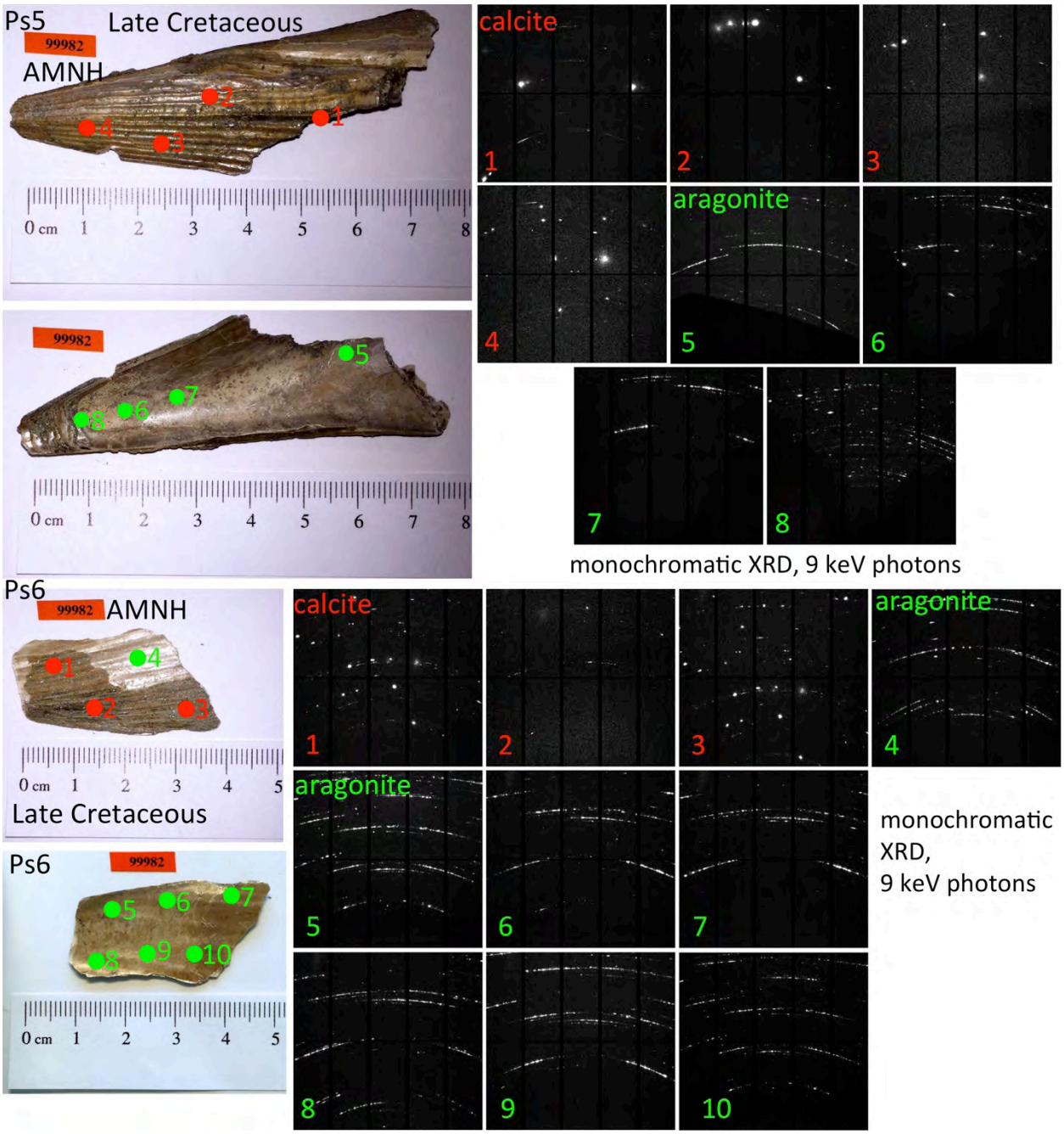

Figure S2. X-ray diffraction patterns, obtained from the red and green spots correspondingly numbered on the photographs. Exterior prismatic layer (top) and interior nacreous layer (bottom) photographs are shown. Indexing demonstrates that in red spot locations the mineral is calcite, and in green spots, aragonite.
Ps5 and Ps6 are the two Late Cretaceous samples in this study, and the only specimens preserving calcite. All other fossil samples contained only aragonite nacre, which was identified as unaltered using spectroscopy at the O K-edge (as in Figure 1) or at the Ca L-edge (DeVol et al., 2014).

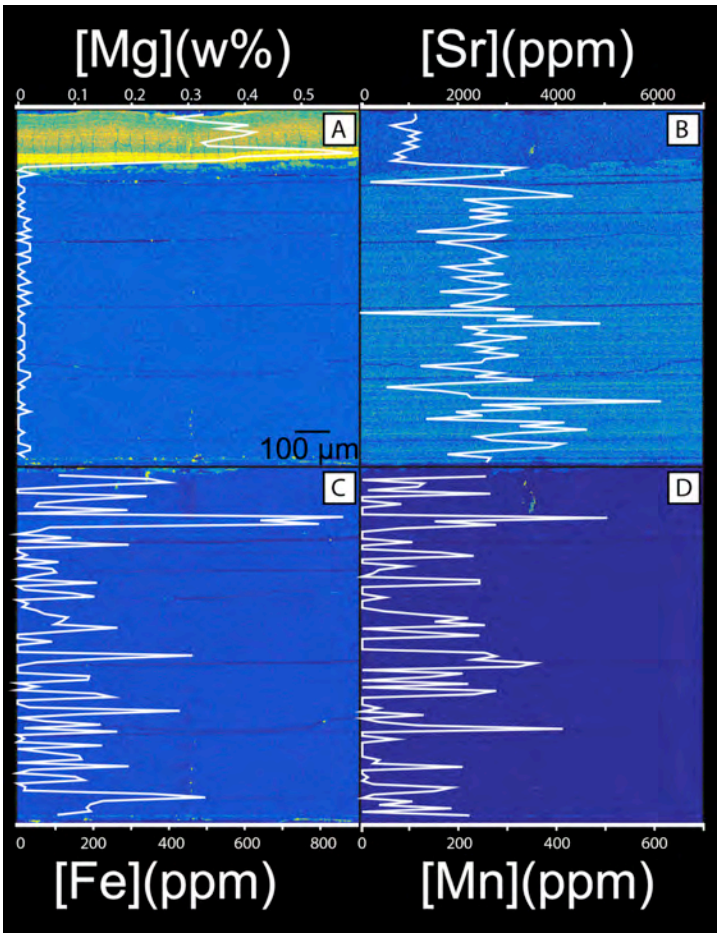

Figure S3. EPMA trace metal maps (with warmer colors indicating higher relative concentration) and quantitative transects (white trace) across one shell sample from the Late Cretaceous (Ps5-4). (A) Mg concentration in units of weight %. (B, C, D) Sr, Fe, Mn concentrations in units of parts per million (ppm). Notice in all images the calcite prismatic layer on top, which appears in yellow, as it is Mg-rich, in panel A, and the rest of the image is nacre with occasional horizontal cracks but otherwise homogeneous elemental distributions.

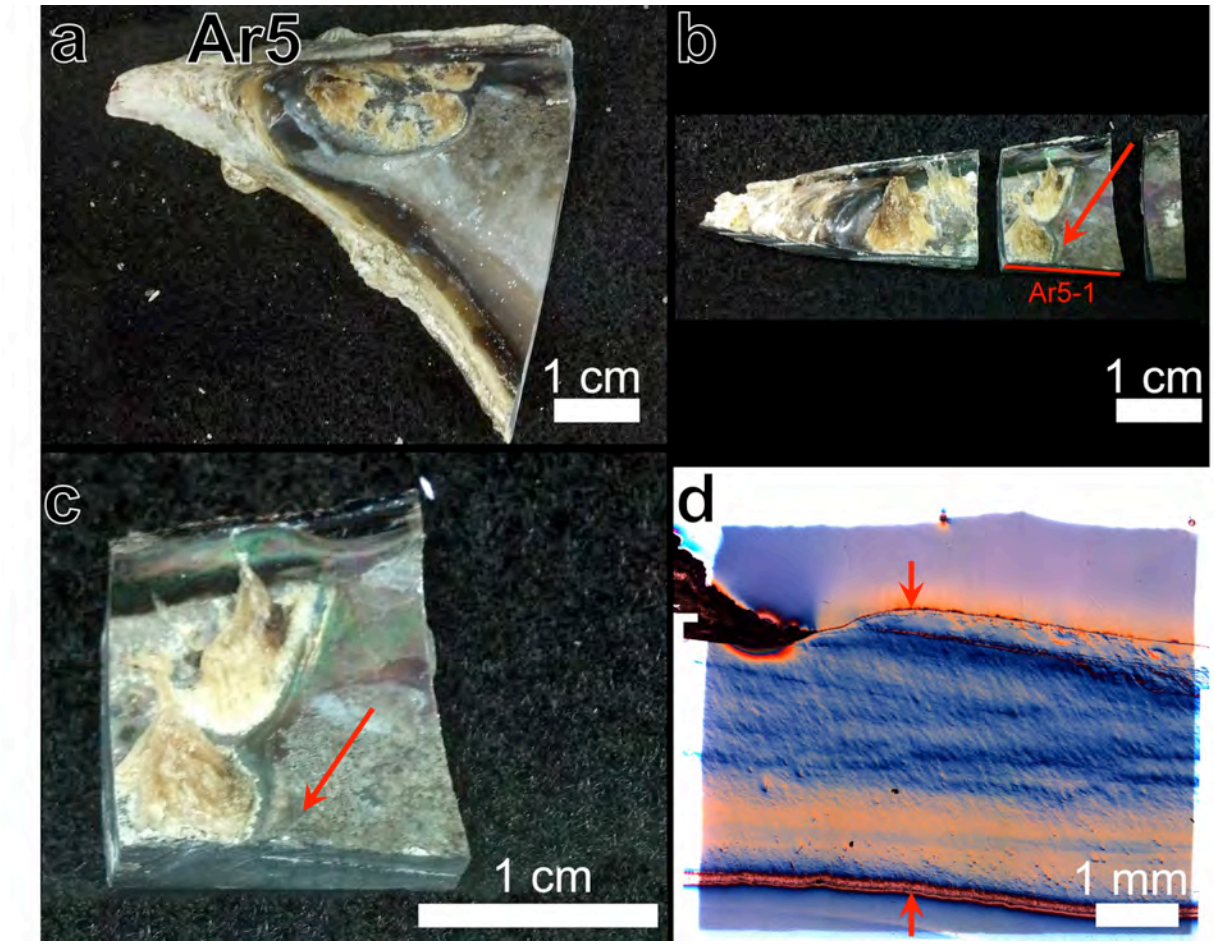

Figure S4. The anterior region of Ar5 shell, modern *Atrina rigida*. (a) The umbo is on the left, thickest nacre is just right of the anterior adductor muscle scars (AAs). Note some remaining organic material on the AAs. (b) The same shell after cutting along the bisector line as well as left and right of sample Ar5-1. The red line indicates the side of the shell fragment to be analyzed. (c) Sample Ar5-1 for PEEM analysis, prior to embedding and polishing. The side of the sample at the bottom of the image will be embedded facing down, and polished. Notice the AAs on the left and the thick nacre (red arrows) at the center of the cross-section. (d) Visible Light Microscopy, Differential Interference Contrast (VLM-DIC) micrograph of sample Ar5-1 cross-section, post embedding, polishing and coating, thus ready for PEEM analysis. In this cross-section the interior of the shell is in the upward direction, the umbo to the left. Notice the AAs on the left, appearing as a depression, and some dark, residual organic matter on the AAs. The thickest part of nacre in this cross-section is between the two red arrows. Complete analysis of this cross-section is shown as a series of overlapping PIC-maps in Figure 6.

Figure S5. Interior and exterior photographs of seven fossil specimens analyzed, prior to sample preparation for PIC-mapping. Note that the umbo, AAs, and region of thickest nacre are well-preserved in most specimens. Whereas all specimens preserve aragonite nacre, prismatic calcite is only preserved in samples Ps5 and Ps6.

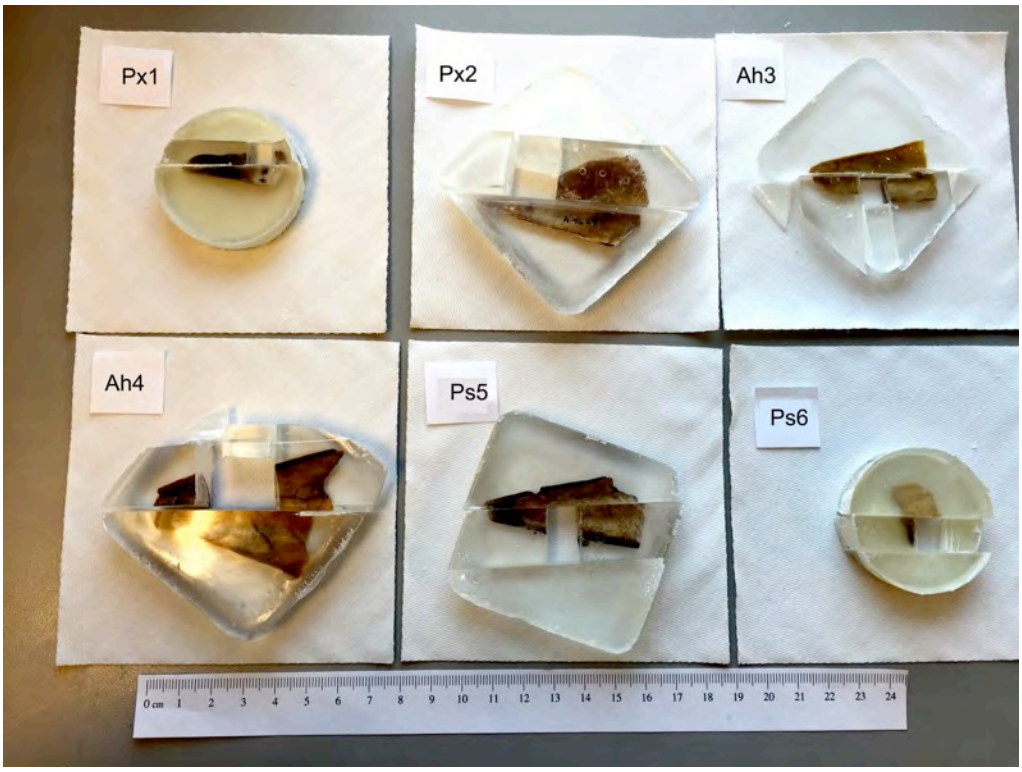

Figure S6. Six of the fossil specimens after the first embedding and cutting (see Figures S7 and S8 for 3 more fossil specimen). All samples are oriented with the interior of the shell facing the reader, and the umbo to the left. The samples analyzed by PEEM are represented by the missing rectangles at the center of each epoxy block. Those are embedded again and polished so the shell transect at the location of thickest nacre is exposed at the center of a flat polished surface, as necessary for the PEEM experiment.

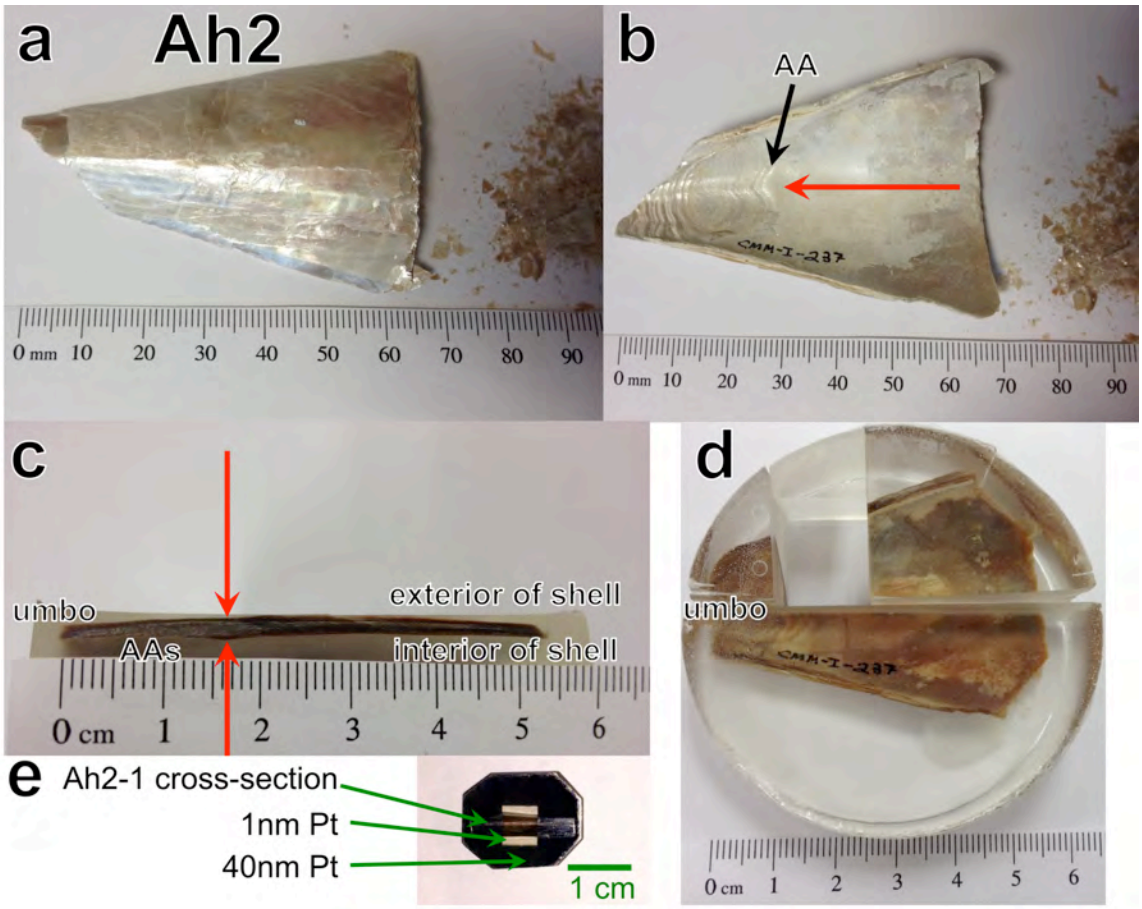

Figure S7. Ah2 sample orientation and preparation. Photographs of the Ah2 shell seen from (a) exterior and (b) interior of the shell. Notice the anterior adductor muscle scar (AA) (black arrow in b) and the thickest nacre (red arrows in b and c) posterior to the umbo with respect to the AAs. The embedded shell was cut as shown in d, re-embedded, then polished and coated to obtain the final sample for PEEM analysis shown in e.

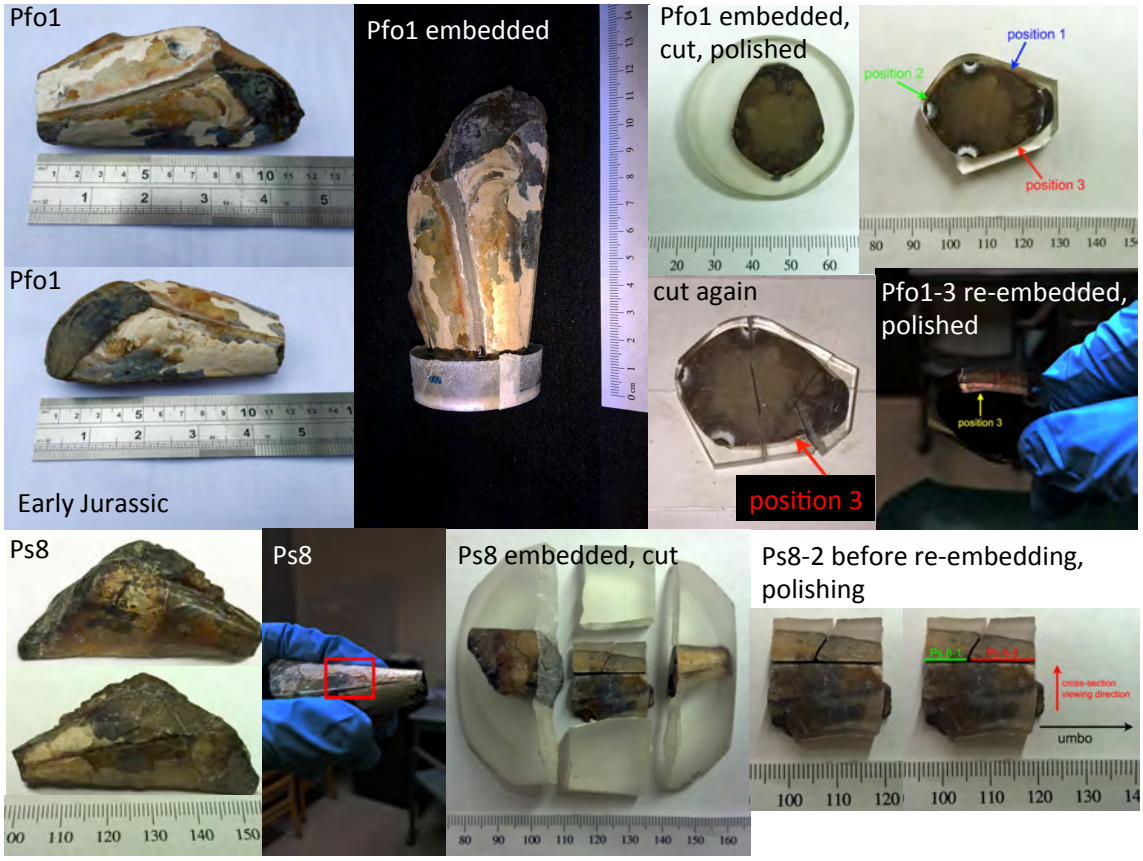

Figure S8. Jurassic specimens *Pinna folium* Pfo1 and *Pinna* sp. Ps8, position of samples Pfo1-3 and Ps8-2, and their preparation. The red arrow (position 3) and the red square indicate the only two regions that still show iridescence in these two ancient shells.

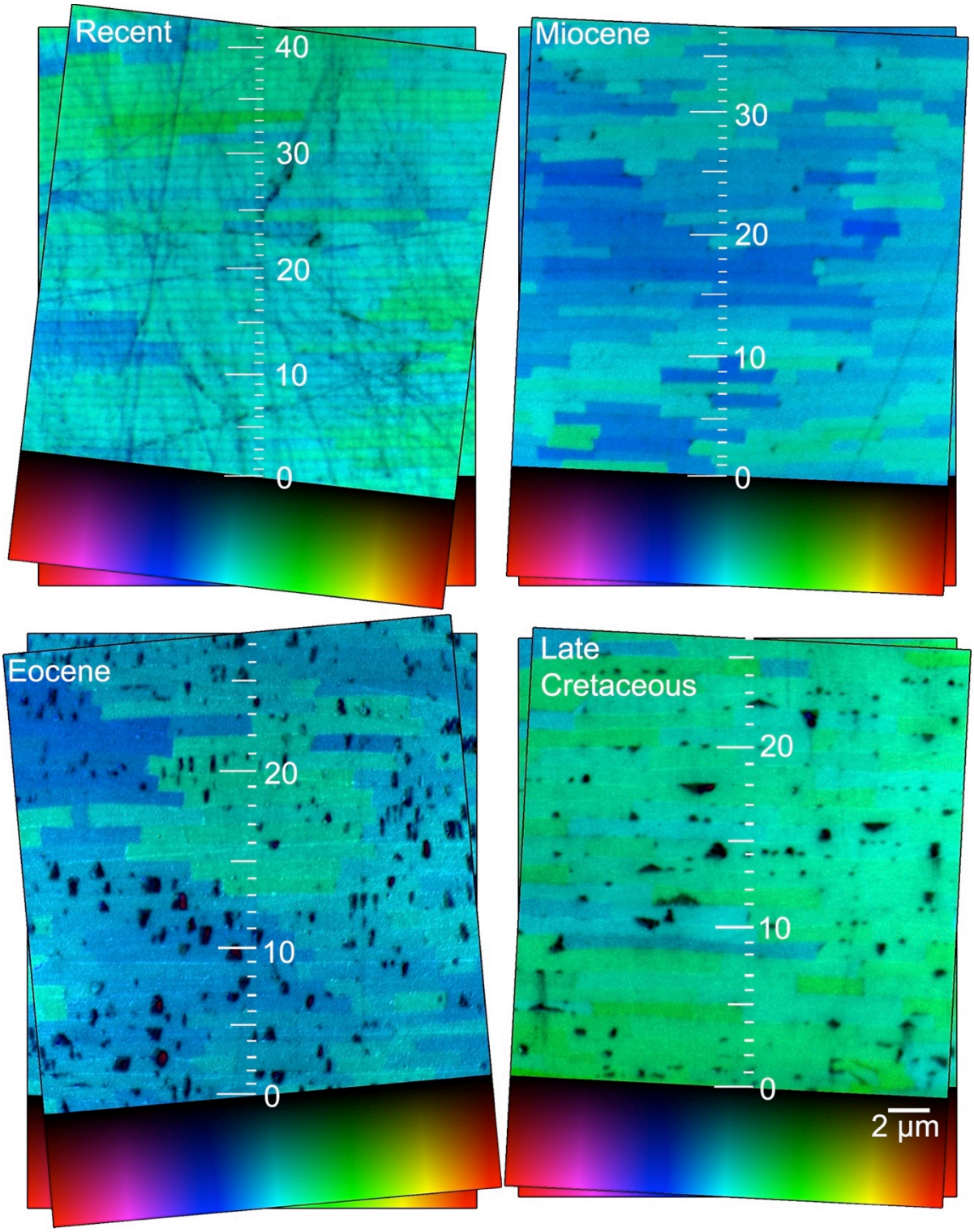

Figure S9. PIC-maps of nacre, including color bar c-axis angles, as they are produced using GG macros (GG–Macros, 2016) for four of the specimen areas illustrated in Figure 3. The samples imaged here are Modern Ar5-1, Miocene Ah4-1, Eocene Px1-1, and Late Cretaceous Ps5-1.

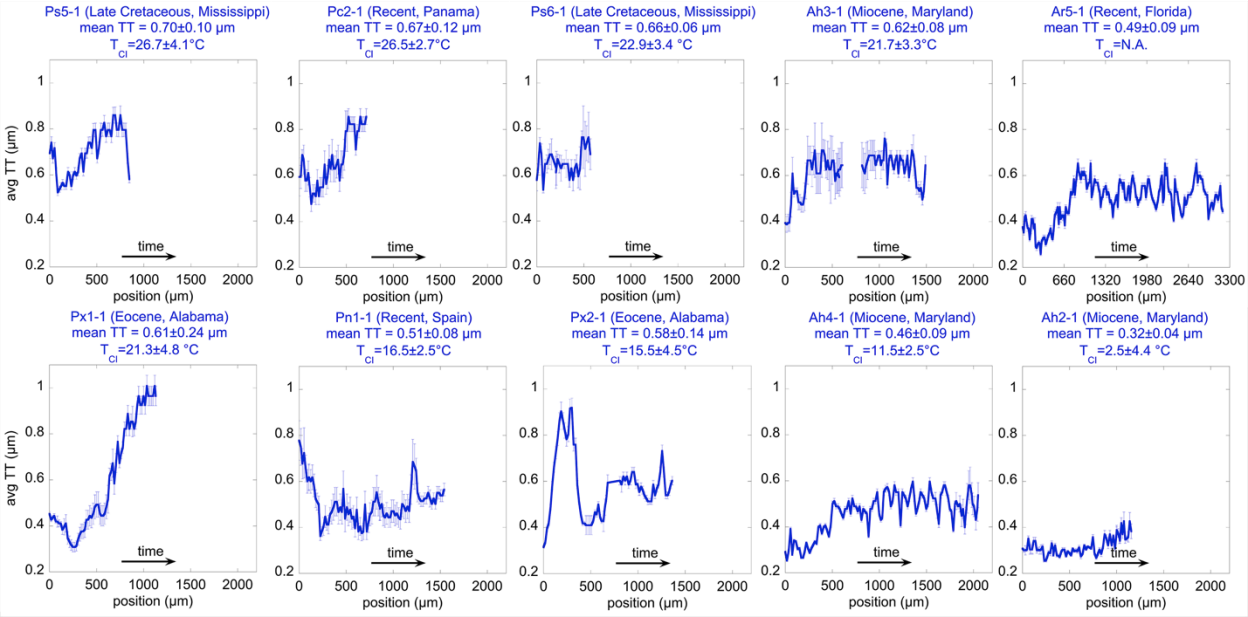

Figure S10. Measurements of nacre tablet thickness (TT) vs. position within each specimen cross-section. In all plots, position is 0 at the oldest (first deposited) nacre layer, and it increases across the thickness of the nacre layer, ending at the interior surface of the shell. Consequently, the "position" axis approximates time of deposition directed left (oldest) to right (youngest). The vertical axis is identical in all plots; the horizontal axis ends at 2200 µm in all plots except Ar5-1, where it ends at 3300 µm to accommodate this shell's thicker nacre layer. The variable in the vertical axis is TT averaged over each image. The mean TT across the entire shell is shown above each plot, ± Standard Deviation. The mean clumped isotope (CI) temperature and its standard error of the mean is also shown at the top of each plot. These are the mean TT and T values plotted in Figure 7B.

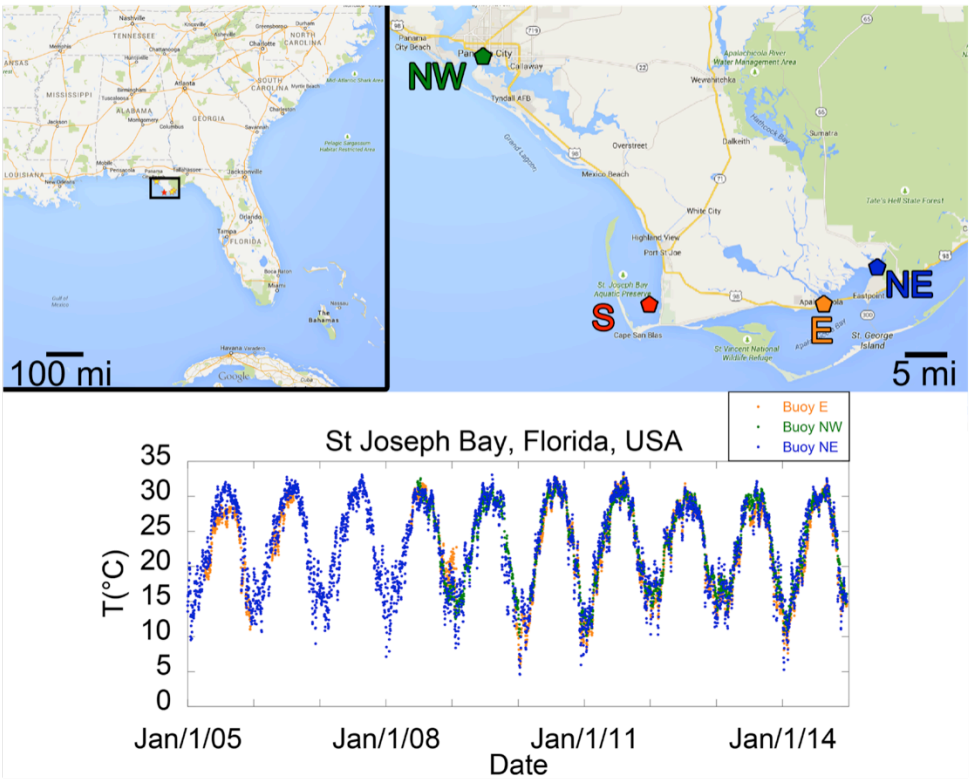

Figure S11. Location of Ar5 and Ar3 shell collection. The right-hand map shows the boxed region from the left panel. S = shell collection site: St. Joseph Bay Aquatic Preserve, Florida, USA. Colored pentagons illustrate the location of three marine weather buoys where T data were collected. Buoys are within 60 km of the shell collection location (S), and T measurements show excellent agreement with one another. The data collection and stations are described on http://www.ndbc.noaa.gov/station_page.php?station=pacf1 , http://www.ndbc.noaa.gov/station_page.php?station=apqf1 , and http://www.ndbc.noaa.gov/station_page.php?station=apcf1 . No clumped isotope data were obtained for samples Ar3 and Ar5.

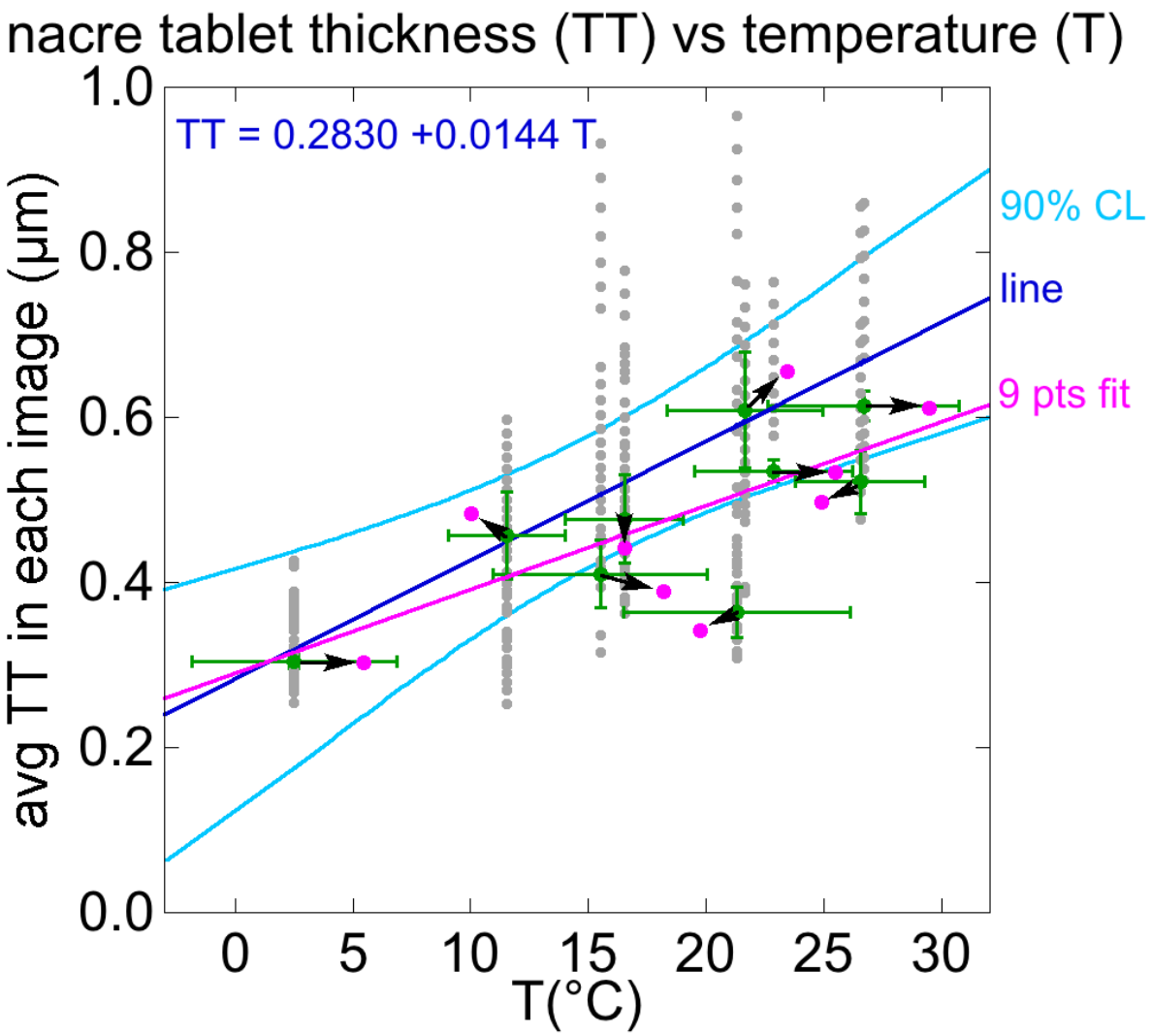

Figure S12. Illustration of the method used for fitting data and evaluating confidence limits. All 630 data points from 9 shells are displayed as grey points. For each trial, we randomly select one point from each shell (green dots), then added random deviates (arrows) within the vertical and horizontal error bars, resulting in 9 new data points (magenta dots). We fitted these 9 data points (magenta line), and repeated 100,000 times. The centroid of the resulting set of 100,000 fit lines is the most probable estimate (blue "line") and the 90th percentile values are the 90% confidence limits (light blue curves).
Error bars for TT measurement, here and in Figure 7A, are 1-5 tablets in each PIC-map, which varied because image quality, sample preservation, and gaps in fossil nacre were all variable across PIC-maps. For T measurements each error bar is one standard error of the mean (S. E. M. = 1 σ /$\sqrt{}$ n, where 1 σ is the StDev of n clumped isotope analyses).

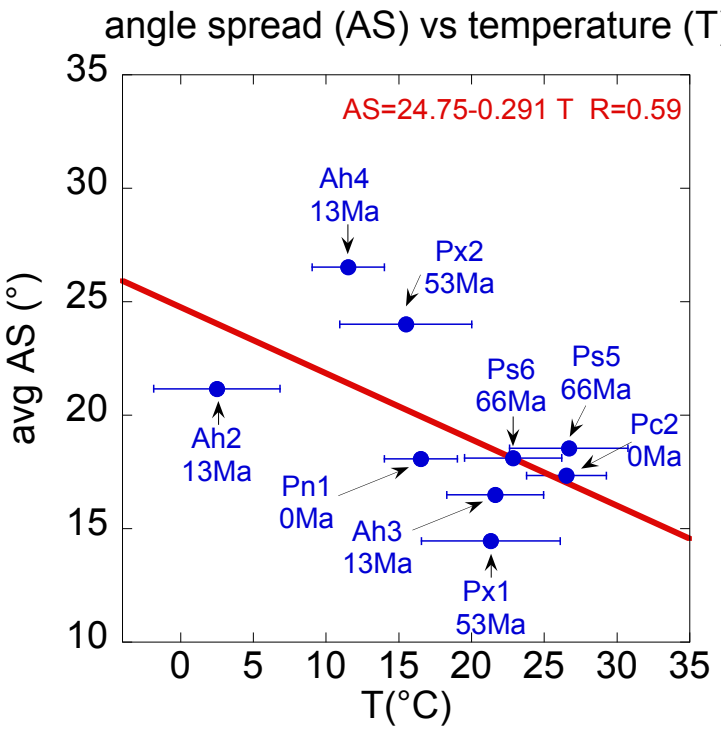

Figure S13. Angle spread (AS) measured in each PIC-map, then averaged over the entire shell. T is measured by clumped isotopes. The relationship of AS and T is weaker than for TT and T, but still acceptable. The negative correlation is possibly due to a sampling artifact: with higher T comes greater TT, so there are fewer crystals per PIC-map, and their AS is smaller.

Table S1

PEEM sample ID	Museum ID	Genus and Species	Epoch	Date of Death	Filenames	# Files	avg TT ± StDev (µm)	avg AS (°)
Pc2-1	MCZ 382622	*Pinna carnea*	Modern	03/2015	Pc2-1-156-188 Pc2-1-189-201	46	0.669 ±0.115	17.3
Ar5-1	Gulf Specimen	*Atrina rigida*	Modern	09/2014	Ar5-1-58-91 Ar5-1-92-125 Ar5-1-126-268 Ar5-1-269-301 Ar5-1-302-333 Ar5-1-334-361	192	0.492 ±0.087	17.2
Pn1-1	MCZ 371544	*Pinna nobilis*	Modern	09/1991	P98-196	117	0.506 ±0.084	18.1
Ah2-1	CMM-I-237	*Atrina harrisii*	Middle Miocene	~12.7-13.2 Ma	Ah2-1-168-206 Ah2-1-206-240	81	0.318 ±0.039	21.2
Ah3-1	YPM 527493	*Atrina harrisii*	Middle Miocene	~12.7-13.2 Ma	Ah3-1-48-86 Ah3-1-87-123 Ah3-1-124-136	89	0.617 ±0.080	16.5
Ah4-1	YPM 527512	*Atrina harrisii*	Middle Miocene	~12.7-13.2 Ma	Ah4-1-125-158 Ah4-1-159-191 Ah4-1-192-225 Ah4-1-225-240	110	0.461 ±0.089	26.5
Px1-1	YPM 527489	*Pinna* sp.	Early Eocene	~52-54 Ma	Px1-1-201-232 Px1-1-233-266	66	0.611 ±0.242	14.4
Px2-1	YPM 527490	*Pinna* sp.	Early Eocene	~52-54 Ma	Px2-1-58-84 Px2-1-84-115 Px2-1-115-123	69	0.580 ±0.141	24.0
Ps5-1	AMNH 99982	*Pinna* sp.	Late Cretaceous	~65.5-66 Ma	Ps5-1-04-37 Ps5-1-38-51	48	0.698 ±0.100	18.5
Ps6-1	AMNH 99982	*Pinna* sp.	Late Cretaceous	~65.5-66 Ma	Ps6-1-21-55	40	0.655 ±0.055	18.1
Pfo1-2	DFM	*Pinna folium*	Early Jurassic	~183-191 Ma	T1 P72-79	8	0.586 ±0.126	-
Pfo1-2	DFM	*Pinna folium*	Early Jurassic	~183-191 Ma	T2 P80-88	9	0.619 ±0.145	-
Ps8-2	LRM	*Pinna sp.*	Early Jurassic	~183-191 Ma	P121-123	3	0.486 ±0.106	-

Table S1. Sample information for the ten *Atrina* and *Pinna* shell samples analyzed in this study. Abbreviations: Gulf Specimen = Gulf Specimen Marine Laboratory, Panacea, FL, USA; MCZ = Museum of Comparative Zoology (MCZ), Harvard University, Cambridge, MA, USA; CMM = Calvert Marine Museum, Solomons, MD, USA; YPD = Yale Peabody Museum of Natural History, Yale University, New Haven, CT, USA; AMNH = American Museum of Natural History, New York, NY, USA; DFM = Dinosaurland Fossil Museum collection, Lyme Regis, UK; LRM = Lyme Regis Museum, Lyme Regis, UK. Filenames correspond to each PIC-map series in Figure S7. An additional modern shell Ar3 (21 cm long) was only used for SEM experiments (Figure 5) and is therefore not listed in this table.

Table S2

Sample ID	Mineralogy	Temperature, °C	Temperature, 1 S.E.M., °C
		Henkes et al., 2012	Carbon Dioxide Equil. Scale
Ah_2	Aragonite	2.51	4.35
Pc_2_2a	Aragonite	26.54	2.73
Pn_1_2a	Aragonite	16.53	2.51
Px_1_2	Aragonite	21.33	4.77
Px_2_2	Aragonite	15.50	4.54
Ah_3_2	Aragonite	21.65	3.33
Ah_4_2	Aragonite	11.54	2.49
Ps_5_2_a	Aragonite	26.70	4.06
Ps_6_2_a	Aragonite	22.87	3.35
Ps_5_2_c	Calcite	23.59	3.41
Ps_6_2_c	Calcite	16.58	1.00

Table S2. Clumped isotope data acquired at Caltech in February 2015, and at MIT in June 2015, with excellent reproducibility between standards and replicates run on both mass spectrometers. Here all data are averaged together, with standard error of the mean (S.E.M.) reported in the last column). Δ_{47} values are reported in the 'carbon dioxide equilibrium scale' based on theoretical equilibrium values of CO_2 (see Dennis et al., 2011 (Dennis et al., 2011)).

Table S3

	Mg (ppm)	Sr (ppm)	Fe (ppm)	Mn (ppm)	S (ppm)
Aragonite Avg.	134	2567	111	90	466
Locations probed	139	139	139	139	139
Std. Error	33	71	12	10	18
Calcite Avg.	3909	986	203	93	1873
Locations probed	21	21	21	21	21
Std. Error	187	38	42	27	195

Table S3. Electron Probe Micro-Analysis (EPMA) data acquired along transects of the Late Cretaceous shell Ps5-4. All 139 data points in nacre aragonite and 21 data points in prismatic calcite are displayed in Figure S3. Here we only show the averages.

Table S4. All 630 data points for the TT vs. T correlation in Figure 7 are presented in Table S4, which is provided as an Excel® file for readers to download and browse. The data columns contain temperature (T) measured by clumped isotopes for each shell, the standard error of the mean (S. E. M.) for T, average Tablet Thickness (TT) in each image, the standard deviation of TT, which varied between 1 and 5 tablets depending on sample and image quality in that image, and the sample identification.

Table S5 shows average values for $\delta^{13}C$, $\delta^{18}O$, Δ_{47} and calculated temperatures.

Table S6 shows the raw, un-averaged, clumped isotope measurements for heated and equilibrated gasses from carbonate standards and shell samples.